Organometallic Oxides: Preparation and Molecular and Electronic Structure of Antiferromagnetic $[(\eta\text{-}C_5H_5)Cr(\mu_3\text{-}O)]_4$ and $[(\eta\text{-}C_5H_5)Cr]_4(\mu_3\text{-}\eta^2\text{-}C_5H_4)(\mu_3\text{-}O)_3$

Frank Bottomley,* Daniel E. Paez, Lori Sutin, and Peter S. White

University of New Brunswick, Fredericton, New Brunswick E3B 5A3, Canada

Frank H. Köhler

Anorganisch-chemisches Institut, Technische Universität München, Lichtenbergstrasse 4, 8046 Garching, Federal Republic of Germany

Robert C. Thompson

Department of Chemistry, University of British Columbia, 2036 Main Mall, Vancouver, British Columbia V6T 1Y6, Canada

Nicholas P. C. Westwood

Department of Chemistry and Biochemistry, Guelph-Waterloo Centre for Graduate Work in Chemistry, University of Guelph, Guelph, Ontario N1G 2W1, Canada

Received March 15, 1990

The reaction between $(\eta\text{-}C_5H_5)_2Cr$ and Me_3NO gave, as the major product, $[(\eta\text{-}C_5H_5)Cr(\mu_3\text{-}O)]_4$ (I) (18%) and, as the minor product (overall isolated yield 2%), $[(\eta\text{-}C_5H_5)Cr]_4(\mu_3\text{-}\eta^2\text{-}C_5H_4)(\mu_3\text{-}O)_3$ (II). I and II were separated by chromatography on glass beads (120–200 mesh). At 295 K I has a distorted (D_2) cubane structure, as determined by X-ray diffraction. The Cr–Cr distances are 2.7114 (6) and 2.7004 (6), 2.8099 (5) and 2.8369 (5), and 2.8933 (5) and 2.8987 (5) Å. The Cr–O–Cr and O–Cr–O angles fall into three sets to conform to the D_2 symmetry, but the Cr–O distances lie in a narrow range, 1.922 (2)–1.947 (2) Å. Crystal data: monoclinic, $P2_1/n$, a = 10.0465 (7) Å, b = 20.9200 (13) Å, c = 10.4345 (4) Å, β = 115.015 (5)°; R = 0.042 for 274 variables and 6022 observed ($I > 2.5\sigma(I)$) reflections with $2\theta < 70°$. The structure was very similar at 100 K. The Cr–Cr distances were 2.6930 (7) and 2.7024 (7), 2.8010 (7) and 2.8270 (7), and 2.8992 (7) and 2.9031 (7) Å; the Cr–O distances were 1.919–1.945 (2) Å. Crystal data: a = 9.9834 (7) Å, b = 20.7828 (23) Å, c = 10.3521 (10) Å, β = 115.359 (7)°; R = 0.028 for 2830 observed reflections with $2\theta < 50°$. In the solid state I is diamagnetic below 50 K and exhibits antiferromagnetic behavior at higher temperatures, the magnetic moment increasing to 3.75 μ_B at 500 K. The magnetic behavior of I has been studied in toluene solution by ^1H and ^{13}C NMR spectroscopy. The observed shifts and their temperature dependence over the temperature range 215–385 K clearly show intramolecular antiferromagnetism. The electron spin delocalization points to magnetic orbitals that are mainly metal in character. The He I photoelectron spectrum in the gas phase at 440 K and the electronic absorption spectrum (450–1550 nm) of a CCl_4 solution of I have been measured; both show considerable low-energy structure. Extended Hückel molecular orbital calculations indicate that the ordering of the 12 nonbonding cluster orbitals for a T_d cubane is $e < a_1 < 1t_2 < t_1 \simeq 2t_2$. The spectra and magnetism of I are interpreted on the basis of a static distortion of a $[(\eta\text{-}C_5H_5)M(\mu_3\text{-}O)]_4$ cubane. The structure of II was previously established by X-ray diffraction as a butterfly cubane derived from I by replacement of a corner oxygen atom with the η^2 ligand C_5H_4

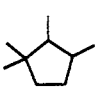

II shows antiferromagnetism between 4 and 120 K. It has a magnetic moment of ca. 2.3 μ_B at 4 K. The magnetic behavior is explained with use of extended Hückel calculations on various forms of I and II; the ground state of the 12 cluster orbitals of II is $1a_2^2 1a_1^2 1b_1^2 1b_2^2 2a_1^2 2b_1^1 3a_1^1$ (in C_{2v} symmetry). The ground state is markedly influenced by the Cr–Cr distance spanned by the η^2-C_5H_4 ligand, because the $2b_1$ orbital is antibonding and the $3a_1$ orbital bonding with respect to this Cr–Cr interaction. II cannot be reduced but is readily oxidized to I by reagents containing oxygen.

Introduction

The first member of the compounds now generically termed "cubanes" was $[CpFe(\mu_3\text{-}S)]_4$ (Cp = η-C_5H_5), independently synthesized and characterized by X-ray diffraction by Dahl[1] and Schunn[2] and co-workers in 1966. Cubanes have interpenetrating tetrahedra of transition metals M and main-group elements A; M and A thus occupy alternate corners of a more or less distorted cube. It is generally agreed that the $[M(\mu_3\text{-}A)]_4$ core of a cubane is held together by normal two-center–two-electron M–A bonds; neither M–M nor A–A bonding is necessary. However, many of the interesting properties of cubanes, such as their detailed structure and magnetic and redox behavior, depend on M–M interactions within the cubane core.

The $[Fe(\mu_3\text{-}S)]_4$ core is now well established in several ferredoxins.[3,4] It has been postulated that a $[MoFe_3(\mu_3\text{-}S)_4]$ cubane, as well as $[Fe(\mu_3\text{-}S)]_4$ cores, are present in nitrogenase.[5,6] In these biochemical systems the ability

(1) Wei, C. H.; Wilkes, G. R.; Treichel, P. M.; Dahl, L. F. *Inorg. Chem.* **1966**, *5*, 900.
(2) Schunn, R. A.; Fritchie, C. J.; Prewitt, C. T. *Inorg. Chem.* **1966**, *5*, 892.
(3) Adman, E. T.; Sieker, L. C.; Jensen, L. H. *J. Biol. Chem.* **1973**, *248*, 3987.
(4) Holm, R. H. *Acc. Chem. Res.* **1977**, *10*, 427.

0276-7333/90/2309-2443$02.50/0

of the $[M(\mu_3\text{-}S)]_4$ core to accept or release electrons without disruption of M–S bonds is crucial to their function. Therefore, the electronic structure of such cubanes is of great interest. In this respect the Cp′ derivatives $[Cp'M(\mu_3\text{-}S)]_4$ (Cp′ = η-C_5R_5), which now exist for M = Ti,[7] V,[7,8] Cr,[9,10] Mo,[11-13] Fe,[1,2,14,15] Ru,[16] and Co,[17] are very important because neither intermolecular interactions between two or more cores nor supporting ligand effects play a significant role in the electronic properties of the core.

All biologically important cubanes contain an $[M(\mu_3\text{-}S)]_4$ core, as do the majority of their $[Cp'M(\mu_3\text{-}A)]_4$ relatives. However, $[Cp'M(\mu_3\text{-}Se)]_4$ cubanes exist,[13,16,18] as do two examples with group 15 elements, $[CpCo(\mu_3\text{-}P)]_4$[19] and $[CpCo(\mu_3\text{-}Sb)]_4$.[20] Only two examples of cubanes containing first-row elements have been reported, these being $[Os(CO)_3(\mu_3\text{-}O)]_4$[21,22] and $[CpCr(\mu_3\text{-}O)]_4$[23,24] (I), though cubane-like cores containing oxygen exist in a number of other materials[25,26] (a list of cubanes is given in ref 11). In fact $[CpCrO]_4$ was prepared in 1960,[27] though it was not recognized as a cubane then. One of the most interesting properties of I is that it is antiferromagnetic, a property not shown by the other $[Cp'M(\mu_3\text{-}A)]_4$ cubanes.

We have previously reported that the reaction between Cp_2Cr and a variety of small molecules containing oxygen (O_2, N_2O, Me_3NO, or C_5H_5NO) gave predominately the dark blue I.[23,24] A small quantity of a green material was also produced.[24] This was shown by X-ray diffraction to be $[CpCr]_4(\mu_3\text{-}\eta^2\text{-}C_5H_4)(\mu_3\text{-}O)_3$ (II).[28] We report here full details of the preparation of II, its magnetic properties, a discussion of its molecular and electronic structure, and a comparison of its physical properties with those of I. We have discussed the structure of I in previous publications[23,24] and have attempted to explain its distortion from T_d symmetry and its antiferromagnetism.[29] The extended Hückel calculations that were the basis of the explanation have been questioned.[11] The structure of $[Cp^1Cr(\mu_3\text{-}O)]_4$ (Cp^1 = η-C_5H_4Me) has been determined recently,[30] and it is so significantly different from I (it has D_{2d} symmetry) that many of the premises on which the original arguments about I were based[29] must be reconsidered. We present here (1) accurate determinations of the structure of I by X-ray diffraction at 295 and 100 K, (2) the magnetic properties of I determined in the solid state over the temperature range 4–500 K and in solution over the range 215–385 K, (3) the He I photoelectron spectrum of I at 440 K in the gas phase, (4) the visible and near-infrared electronic spectrum of I in CCl_4 solution, (5) new extended Hückel molecular orbital calculations on various forms of I (of T_d, D_{2d}, D_2, and C_{2v} symmetries), and (6) other physical and chemical properties that provide information on the electronic structure of the $[Cr(\mu_3\text{-}O)]_4$ core of I.

Experimental Section

General Considerations. All operations were conducted under argon or vacuum. All glassware was oven- and then flame-dried under vacuum. Toluene, ether, and tetrahydrofuran (THF) were predried with use of Na or $LiAlH_4$, stored over MeLi under vacuum, and distilled directly onto the reagents under vacuum. The starting material Cp_2Cr was prepared by the literature method;[31] Me_3NO was purchased from Sigma-Aldrich and purified by sublimation at 70 °C under vacuum. The product II was separated from I by using a chromatography column designed to attach to the vacuum line. The column had side arms with greaseless stopcocks at both the top and the bottom. The glass-bead support, the reaction mixture, and the eluting solvents were all added while maintaining an argon purge through the column. The rate of eluent flow and the removal of fractions were controlled by the side-arm stopcocks and by side-arm flasks above and below the column.

Preparation of $[CpCr(\mu_3\text{-}O)]_4$ (I) and $[CpCr]_4(\mu_3\text{-}\eta^2\text{-}C_5H_4)(\mu_3\text{-}O)_3$ (II). A solution of Cp_2Cr (10.05 g, 55 mmol) and Me_3NO (1.38 g, 18.4 mmol) in toluene (100 cm^3) was stirred at room temperature for 25 h. The resultant blue-green solution was filtered and the solvent reduced to approximately 10 cm^3. The solution was chromatographed on glass beads (PG-240-200, mesh size 120-200). The eluents were ether and THF, beginning with pure ether and gradually increasing the amount of THF during the separation. A red band of unreacted Cp_2Cr eluted first, followed by a blue band of $[CpCr(\mu_3\text{-}O)]_4$ (I). Finally, with pure THF as eluent, a green band of $[CpCr]_4(\mu_3\text{-}\eta^2\text{-}C_5H_4)(\mu_3\text{-}O)_3$ (II) was obtained. The THF was removed in vacuo. The residue was washed with cold hexane and then recrystallized from toluene, yielding green II (0.10 g, 0.17 mmol; 2% yield based on the Cp_2Cr actually used in the reaction). The solvent mixture was removed from the blue band of I in vacuo and the residue recrystallized from toluene; yield of I 1.31 g, 2.47 mmol, 18%.

Characterization of I. Anal. Calcd for $C_{20}H_{20}Cr_4O_4$: C, 45.1; H, 3.8; Cr, 39.1. Found: C, 44.9; H, 4.0; Cr (as Cr_2O_3), 39.3. Mass spectrum (EI, 70 eV): m/e 532 ($[M]^+$), 467 ($[M - (C_5H_5)]^+$), 402 ($[M - 2(C_5H_5)]^+$), 350 ($[(C_5H_5)_2Cr_3O_4]^+$), 337 ($[M - 3(C_5H_5)]^+$), 272 ($[Cr_4O_4]^+$), 266 ($[(C_5H_5)_2Cr_2O_2]^+$), 204 ($[Cr_3O_3]^+$), 182 ($[(C_5H_5)_2Cr]^+$). Infrared spectrum (cm^{-1}): 3062 (m, ν(C–H)); 1438 (m, ν(C–C)); 1018 (s, ϑ(CH)); 794 (vs, π(CH)); 590 (s, π(CH)); 555

(5) Holm, R. H. *Chem. Soc. Rev.* **1981**, *10*, 455.
(6) Schultz, F. A.; Gheller, S. F.; Burgess, B. K.; Lough, S.; Newton, W. E. *J. Am. Chem. Soc.* **1985**, *107*, 5364.
(7) Darkwa, J.; Lockemeyer, J. R.; Boyd, P. D. W.; Rauchfuss, T. B.; Rheingold, A. L. *J. Am. Chem. Soc.* **1988**, *110*, 141.
(8) Eremenko, I. L.; Pasynskii, A. A.; Katugin, A. S.; Ellert, O. G.; Shklover, V. E.; Struchkov, Yu. T. *Bull. Acad. Sci. USSR, Div. Chem. Sci. (Engl. Transl.)* **1984**, 1531.
(9) Pasynskii, A. A.; Eremenko, I. L.; Orazsakhatov, B.; Kalinnikov, V. T.; Aleksandrov, G. G.; Struchkov, Yu. T. *J. Organomet. Chem.* **1981**, *216*, 211.
(10) Pasynskii, A. A.; Eremenko, I. L.; Rakitin, Y. V.; Novotortsev, V. M.; Ellert, O. G.; Kalinnikov, V. T.; Shklover, V. E.; Struchkov, Yu. V.; Lindeman, S. V.; Kurbanov, T. K.; Gasanov, G. S. *J. Organomet. Chem.* **1983**, *248*, 309.
(11) Williams, P. D.; Curtis, M. D. *Inorg. Chem.* **1986**, *25*, 4562.
(12) Bandy, J. A.; Davies, C. E.; Green, J. C.; Green, M. L. H.; Prout, K.; Rodgers, D. P. S. *J. Chem. Soc., Chem. Commun.* **1983**, 1395.
(13) Green, M. L. H.; Hamnett, A.; Qin, J.; Baird, P.; Bandy, J. A.; Prout, K.; Marseglia, E.; Obertelli, S. D. *J. Chem. Soc., Chem. Commun.* **1987**, 1811.
(14) Trinh-Toan; Teo, B. K.; Ferguson, J. A.; Meyer, T. J.; Dahl, L. F. *J. Am. Chem. Soc.* **1977**, *99*, 408.
(15) Trinh-Toan; Fehlhammer, W. P.; Dahl, L. F. *J. Am. Chem. Soc.* **1977**, *99*, 402.
(16) Amarasekera, J.; Rauchfuss, T. B.; Wilson, S. R. *J. Chem. Soc., Chem. Commun.* **1989**, 14.
(17) Simon, G. L.; Dahl, L. F. *J. Am. Chem. Soc.* **1973**, *95*, 2164.
(18) Ogino, H.; Tobita, H.; Yanagisawa, K.; Shimoi, M.; Kabuto, C. *J. Am. Chem. Soc.* **1987**, *109*, 5847.
(19) Simon, G. L.; Dahl, L. F. *J. Am. Chem. Soc.* **1973**, *95*, 2175.
(20) Foust, A. S.; Dahl, L. F. *J. Am. Chem. Soc.* **1970**, *92*, 7337.
(21) Johnson, B. F. G.; Lewis, J.; Williams, I. G.; Wilson, J. *J. Chem. Soc., Chem. Commun.* **1966**, 391.
(22) Bright, D. A. *J. Chem. Soc., Chem. Commun.* **1970**, 1169.
(23) Bottomley, F.; Paez, D. E.; White, P. S. *J. Am. Chem. Soc.* **1981**, *103*, 5581.
(24) Bottomley, F.; Paez, D. E.; White, P. S. *J. Am. Chem. Soc.* **1982**, *104*, 5651.
(25) Haushalter, R. C. *J. Chem. Soc., Chem. Commun.* **1987**, 1566.
(26) McKee, V.; Shepard, W. B. *J. Chem. Soc., Chem. Commun.* **1985**, 158.
(27) Fischer, E. O.; Ulm, K.; Fritz, H. P. *Chem. Ber.* **1960**, *93*, 2167.
(28) Bottomley, F.; Paez, D. E.; Sutin, L.; White, P. S. *J. Chem. Soc., Chem. Commun.* **1985**, 597.
(29) Bottomley, F.; Grein, F. *Inorg. Chem.* **1982**, *21*, 4170.
(30) Eremenko, I. L.; Nefedov, S. E.; Pasynskii, A. A.; Orazsakhatov, B.; Ellert, O. G.; Struchkov, Yu. T.; Yanovsky, A. I.; Zagorevsky, D. V. *J. Organomet. Chem.* **1989**, *368*, 185.
(31) King, R. B. *Organometallic Synthesis of Air Sensitive Compounds*; McGraw-Hill: New York, 1969.

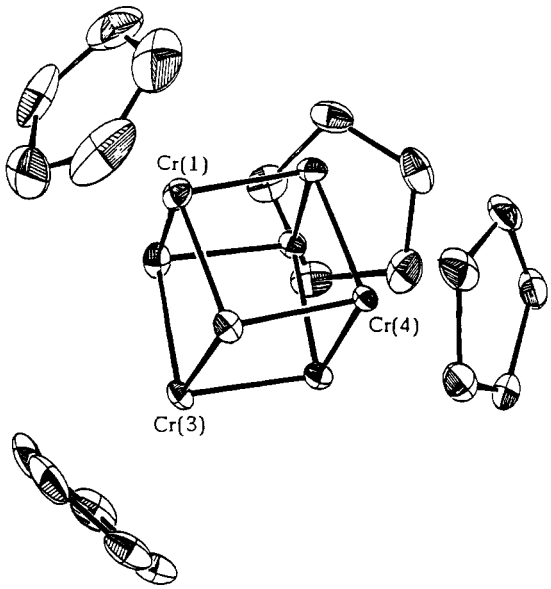

Figure 1. ORTEP plot of $[CpCr(\mu_3\text{-}O)]_4$ (I) at 295 K (hydrogen atoms omitted for clarity).

(m, $\nu([Cr(\mu_3\text{-}O)]_4)$). ^1H NMR ($(^2H_8)$toluene solution, 200 MHz, 295 K): −36.10 ppm relative to TMS (v br singlet).

Characterization of II. Anal. Calcd for $C_{32}H_{32}Cr_4O_3$ ($[(C_5H_5)Cr]_4(C_5H_4)O_3{\cdot}C_6H_5CH_3$): C, 57.1; H, 4.8; Cr, 30.9. Found (two different samples): C, 56.6, 56.6; H, 5.1, 4.8; Cr (as Cr_2O_3) 30.2. Mass spectrum (EI, 70 eV): m/e 580 (M^+; intensity relative to 100 for C_5H_6, 7.5), 515 ($[M - C_5H_5]^+$, 4.0), 467 ($[(C_5H_5)_3Cr_4O_4]^+$, 2.8), 449 ($[M - 2C_5H_5 - H]^+$, 10.0), 431 ($[(C_5H_5)_3Cr_3O(C_5H_4)]^+$, 0.8), 398 ($[(C_5H_5)_2Cr_3(C_5H_4)O_3]^+$, 2.3), 384 ($[(C_5H_5)Cr_4O_3(C_5H_3)]^+$, 1.3), 381 ($[(C_5H_5)_2Cr_3(C_5H_3)O_2]^+$, 1.0), 366 ($[(C_5H_5)_2Cr_3O(C_5H_4)]^+$, 0.5), 332 ($[(C_5H_5)Cr_3O_3(C_5H_3)]^+$, 1.0), 316 ($[(C_5H_5)Cr_3O_2(C_5H_3)]^+$, 2.8). Infrared spectrum (KBr disk, cm^{-1}): ν(C–H) 3025 (w), 2958 (m), 2928 (m), 2870 (m); ν_{asym}(Cr–O) 575. ^1H NMR ($(^2H_8)$toluene solution, 200 MHz): +2.9 ppm (very broad, very weak). The ESR spectrum showed no signal at room temperature or at 90 K. The X-ray data were reported previously.[28] The magnetic behavior is shown in Figure 13.

X-ray Diffraction Experiments. The structure of I was determined at 295 and 100 K with use of the same crystal, of dimensions 0.25 × 0.25 × 0.25 mm. Preliminary photographic and diffractometric investigation confirmed the previous crystal data.[24] The larger data set and number of reflections used in refinement of the cell parameters mean that the data quoted below are significantly more accurate than those reported previously.

Crystal Data at 295 K: $C_{20}H_{20}Cr_4O_4$, M_r = 532.35, monoclinic, $P2_1/n$, a = 10.0465 (7) Å, b = 20.9200 (13) Å, c = 10.4345 (4) Å, β = 115.015 (5)°, V = 1987.3 (2) Å^3, Z = 4, D_x = 1.78 Mg m^{-3}, Mo Kα radiation (λ = 0.709 30 Å), μ(Mo Kα) = 21.0 cm^{-1}. Cell dimensions were obtained from 55 reflections with $40 < 2\theta < 50°$.

Crystal Data at 100 K: a = 9.9834 (7) Å, b = 20.7828 (23) Å, c = 10.3521 (10) Å, β = 115.359 (7)°, V = 1940.9 (3) Å^3. Cell dimensions were obtained from 50 reflections with $30 < 2\theta < 45°$.

Data Collection. An Enraf-Nonius CAD4 diffractometer was run under the control of the NRCCAD program[32] (scan mode $\theta/2\theta$). At 295 K 33 509 reflection intensities were measured to $2\theta_{max}$ = 70° and averaged to yield 8672 unique reflections, of which 6022 were regarded as observed ($I > 2.5\sigma(I)$). The data were corrected for absorption by empirical methods (DIFABS[33]). At 100 K 12 174 reflection intensities were measured to $2\theta_{max}$ = 50° and averaged to yield 3220 unique reflections, of which 2830 had $I > 2.5\sigma(I)$. DIFABS[33] was applied.

Refinement at 295 K. The NRCVAX program suite[34] was used; scattering factors were taken from ref 35 and corrected for anomalous dispersion. All non-hydrogen atoms were refined anisotropically. The H atoms were included with a fixed C–H distance of 0.96 Å and variable isotropic thermal parameters. An extinction parameter was refined, for a total of 274 variables. The final residuals were R ($\sum(|F_o| - |F_c|)/\sum|F_o|$) = 0.042, R_w ($=[\sum w(|F_o| - |F_c|)^2/\sum w(|F_o|)^2]^{1/2}$) = 0.054, and GOF ($=[\sum w(|F_o| - |F_c|)^2/((\text{no. of reflections}) - (\text{no. of parameters}))]^{1/2}$) = 1.209. The maximum Δ/σ in the final cycle was 0.86. A final difference Fourier synthesis had a maximum peak of 0.680 e Å^{-3} near a C atom of the C_5H_5 ring attached to Cr(1) and a minimum hole of −0.680 e Å^{-3}. The final positional parameters for the non-hydrogen atoms are given

Table I. Atomic Parameters x, y, and z and B_{iso} for the Non-Hydrogen Atoms of $[CpCr(\mu_3\text{-}O)]_4$ at 295 K (Esd's in Parentheses)

	x	y	z	B_{iso},[a] Å^2
Cr(1)	0.74787 (4)	0.418812 (18)	0.63263 (4)	1.290 (14)
Cr(2)	0.70073 (4)	0.379696 (17)	0.35068 (4)	1.064 (14)
Cr(3)	0.70837 (4)	0.293159 (18)	0.56299 (4)	1.030 (13)
Cr(4)	0.96431 (4)	0.359705 (17)	0.56971 (4)	1.039 (13)
O(1)	0.86914 (18)	0.34381 (8)	0.69348 (17)	1.17 (6)
O(2)	0.83534 (18)	0.43260 (7)	0.50128 (17)	1.16 (7)
O(3)	0.60350 (19)	0.37071 (8)	0.47630 (17)	1.34 (7)
O(4)	0.81014 (18)	0.30410 (8)	0.44201 (17)	1.16 (6)
C(11)	0.8133 (5)	0.45104 (22)	0.8569 (3)	4.66 (19)
C(12)	0.6652 (5)	0.43423 (18)	0.7989 (4)	4.17 (22)
C(13)	0.5901 (4)	0.47643 (20)	0.6886 (4)	3.91 (18)
C(14)	0.6862 (5)	0.51823 (17)	0.6760 (4)	4.03 (20)
C(15)	0.8249 (5)	0.50382 (20)	0.7788 (4)	4.45 (21)
C(21)	0.5644 (3)	0.34789 (13)	0.1257 (3)	2.00 (11)
C(22)	0.5095 (3)	0.40777 (13)	0.1435 (3)	1.94 (11)
C(23)	0.6213 (3)	0.45369 (13)	0.1740 (3)	2.04 (12)
C(24)	0.7456 (3)	0.42235 (15)	0.1742 (3)	2.33 (12)
C(25)	0.7108 (3)	0.35740 (15)	0.1436 (3)	2.27 (12)
C(31)	0.5210 (3)	0.25110 (16)	0.5981 (4)	2.97 (15)
C(32)	0.6504 (4)	0.24551 (16)	0.7249 (3)	2.97 (15)
C(33)	0.7471 (3)	0.20432 (13)	0.7002 (3)	2.28 (11)
C(34)	0.6784 (3)	0.18510 (13)	0.5593 (3)	2.18 (12)
C(35)	0.5388 (3)	0.21387 (14)	0.4951 (3)	2.52 (11)
C(41)	1.1345 (3)	0.36734 (14)	0.4843 (3)	2.15 (12)
C(42)	1.1528 (3)	0.30801 (13)	0.5539 (3)	2.11 (12)
C(43)	1.1912 (3)	0.31997 (14)	0.6978 (3)	2.17 (11)
C(44)	1.1966 (3)	0.38734 (14)	0.7162 (3)	2.27 (11)
C(45)	1.1621 (3)	0.41626 (13)	0.5839 (3)	2.23 (12)

[a] B_{iso} is the mean of the principal axes of the thermal ellipsoid.

Table II. Important Distances (Å) and Angles (deg) in $[CpCr(\mu_3\text{-}O)]_4$ at 295 K (Esd's in Parentheses)

Cr(1)–Cr(2)	2.8933 (5)	Cr(2)–O(4)	1.932 (2)
Cr(1)–Cr(3)	2.7114 (6)	Cr(3)–O(1)	1.930 (2)
Cr(1)–Cr(4)	2.8099 (5)	Cr(3)–O(3)	1.938 (2)
Cr(2)–Cr(3)	2.8369 (5)	Cr(3)–O(4)	1.945 (2)
Cr(2)–Cr(4)	2.7004 (6)	Cr(4)–O(1)	1.933 (2)
Cr(3)–Cr(4)	2.8987 (5)	Cr(4)–O(2)	1.932 (2)
Cr(1)–O(1)	1.922 (2)	Cr(4)–O(4)	1.945 (2)
Cr(1)–O(2)	1.937 (2)	Cr(1)–Cp[a]	1.922 (2)
Cr(1)–O(3)	1.943 (2)	Cr(2)–Cp	1.922 (2)
Cr(2)–O(2)	1.930 (2)	Cr(3)–Cp	1.920 (2)
Cr(2)–O(3)	1.947 (2)	Cr(4)–Cp	1.908 (2)
O(1)–Cr(1)–O(2)	86.65 (7)	Cr(1)–O(1)–Cr(3)	89.47 (7)
O(1)–Cr(1)–O(3)	89.91 (7)	Cr(1)–O(1)–Cr(4)	93.57 (7)
O(2)–Cr(1)–O(3)	83.34 (7)	Cr(3)–O(1)–Cr(4)	97.24 (7)
O(2)–Cr(2)–O(3)	83.42 (7)	Cr(1)–O(2)–Cr(2)	96.85 (7)
O(2)–Cr(2)–O(4)	90.64 (7)	Cr(1)–O(2)–Cr(4)	93.15 (7)
O(3)–Cr(2)–O(4)	86.08 (7)	Cr(2)–O(2)–Cr(4)	88.73 (7)
O(1)–Cr(3)–O(3)	89.85 (7)	Cr(1)–O(3)–Cr(2)	96.10 (8)
O(1)–Cr(3)–O(4)	83.14 (7)	Cr(1)–O(3)–Cr(3)	88.64 (7)
O(3)–Cr(3)–O(4)	85.97 (7)	Cr(2)–O(3)–Cr(3)	93.82 (7)
O(1)–Cr(4)–O(2)	86.49 (7)	Cr(2)–O(4)–Cr(3)	94.07 (7)
O(1)–Cr(4)–O(4)	83.06 (7)	Cr(2)–O(4)–Cr(4)	88.31 (7)
O(2)–Cr(4)–O(4)	90.20 (7)	Cr(3)–O(4)–Cr(4)	96.35 (7)

[a] Cp is the centroid of the C_5H_5 ring.

(32) LePage, Y.; White, P. S.; Gabe, E. J. Annual Meeting of the American Crystallographic Association, Hamilton, Ontario, Canada, 1986.
(33) Walker, N.; Stuart, D. *Acta Crystallogr.* **1983**, *A39*, 158.
(34) Gabe, E. J.; Lee, F. L.; LePage, Y. In *Crystallographic Computing*; Sheldrick, G. M., Kruger, C., Goddard, R., Eds.; Clarendon: Oxford, U.K., 1985; Vol. 3, p 167.
(35) *International Tables for X-ray Crystallography*; Kynoch Press: Birmingham, U.K., 1974; Vol. IV.

Table III. Atomic Parameters x, y, and z and B_{iso} for the Non-Hydrogen Atoms of $[CpCr(\mu_3\text{-}O)]_4$ at 100 K (Esd's in Parentheses)

	x	y	z	B_{iso},[a] Å^2
Cr(1)	0.74556 (5)	0.419218 (23)	0.63406 (5)	1.138 (20)
Cr(2)	0.69815 (5)	0.378547 (22)	0.34978 (5)	1.018 (20)
Cr(3)	0.70684 (5)	0.292967 (23)	0.56550 (5)	0.996 (19)
Cr(4)	0.96409 (5)	0.360682 (22)	0.57222 (5)	1.020 (20)
O(1)	0.86900 (22)	0.34424 (10)	0.69669 (21)	1.13 (8)
O(2)	0.83210 (22)	0.43326 (10)	0.50085 (21)	1.15 (9)
O(3)	0.60006 (23)	0.37066 (10)	0.47585 (21)	1.22 (9)
O(4)	0.81073 (22)	0.30319 (10)	0.44519 (21)	1.09 (9)
C(11)	0.8297 (4)	0.50291 (19)	0.7876 (4)	2.64 (18)
C(12)	0.6902 (5)	0.51975 (17)	0.6794 (4)	2.48 (18)
C(13)	0.5860 (4)	0.47764 (18)	0.6870 (4)	2.23 (16)
C(14)	0.6584 (4)	0.43449 (18)	0.7989 (4)	2.35 (18)
C(15)	0.8100 (4)	0.45053 (20)	0.8611 (4)	2.73 (17)
C(21)	0.7096 (4)	0.35503 (16)	0.1420 (3)	1.74 (14)
C(22)	0.5603 (3)	0.34591 (15)	0.1225 (3)	1.51 (14)
C(23)	0.5067 (3)	0.40661 (16)	0.1393 (3)	1.51 (13)
C(24)	0.6187 (4)	0.45251 (15)	0.1699 (3)	1.55 (14)
C(25)	0.7444 (4)	0.42049 (16)	0.1723 (3)	1.69 (14)
C(31)	0.7477 (4)	0.20369 (15)	0.7051 (3)	1.66 (14)
C(32)	0.6521 (4)	0.24597 (16)	0.7319 (3)	1.84 (14)
C(33)	0.5200 (4)	0.25196 (16)	0.6055 (4)	2.00 (16)
C(34)	0.5337 (3)	0.21375 (16)	0.4991 (3)	1.73 (14)
C(35)	0.6740 (4)	0.18445 (16)	0.5608 (3)	1.65 (14)
C(41)	1.1987 (3)	0.38870 (16)	0.7210 (3)	1.65 (14)
C(42)	1.1931 (3)	0.32118 (16)	0.7021 (3)	1.54 (14)
C(43)	1.1539 (3)	0.30942 (16)	0.5569 (4)	1.59 (15)
C(44)	1.1348 (3)	0.36887 (16)	0.4861 (3)	1.57 (14)
C(45)	1.1630 (3)	0.41825 (15)	0.5877 (4)	1.64 (14)

[a] B_{iso} is the mean of the principal axes of the thermal ellipsoid.

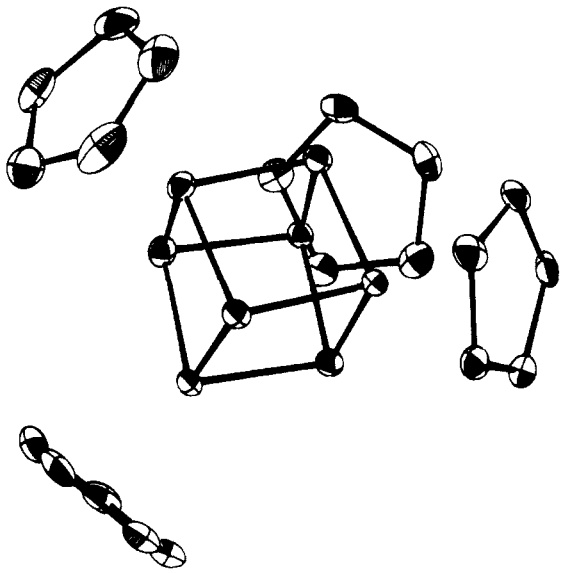

Figure 2. ORTEP plot of $[CpCr(\mu_3\text{-}O)]_4$ (I) at 100 K (hydrogen atoms omitted for clarity).

in Table I, important derived distances and angles are in Table II, and an ORTEP[36] plot of the molecule is given in Figure 1. The H atom positional parameters, the anisotropic (for C, Cr, and O) and isotropic (for H) thermal parameters, a complete table of distances and angles, some mean planes, and a table of $|F_o|$ and $|F_c|$ are available in the supplementary material.

Refinement at 100 K: $R = 0.028$, $R_w = 0.040$, GOF = 1.420, maximum Δ/σ 0.341, maximum peak in final difference map 0.370 e Å^{-3}, minimum hole −0.360 e Å^{-3}. The final positional parameters for C, Cr, and O are given in Table III, derived important distances and angles are in Table IV, and an ORTEP plot is given in Figure 2. Other details are available as for the refinement at 295 K.

(36) Johnson, C. K. ORTEP-II: A FORTRAN Thermal Ellipsoid Plot Program for Crystal Structure Illustrations. Report ORNL-5138; Oak Ridge National Laboratory: Oak Ridge, TN, 1976.

Table IV. Important Distances (Å) and Angles (deg) in $[CpCr(\mu_3\text{-}O)]_4$ at 100 K (Esd's in Parentheses)

Cr(1)-Cr(2)	2.8992 (7)	Cr(2)-O(4)	1.934 (2)
Cr(1)-Cr(3)	2.7024 (7)	Cr(3)-O(1)	1.928 (2)
Cr(1)-Cr(4)	2.8010 (7)	Cr(3)-O(3)	1.938 (2)
Cr(2)-Cr(3)	2.8270 (7)	Cr(3)-O(4)	1.944 (2)
Cr(2)-Cr(4)	2.6930 (7)	Cr(4)-O(1)	1.930 (2)
Cr(3)-Cr(4)	2.9031 (7)	Cr(4)-O(2)	1.930 (2)
Cr(1)-O(1)	1.919 (2)	Cr(4)-O(4)	1.943 (2)
Cr(1)-O(2)	1.937 (2)	Cr(1)-Cp[a]	1.914 (2)
Cr(1)-O(3)	1.942 (2)	Cr(2)-Cp	1.920 (2)
Cr(2)-O(2)	1.933 (2)	Cr(3)-Cp	1.918 (2)
Cr(2)-O(3)	1.945 (2)	Cr(4)-Cp	1.906 (3)
O(1)-Cr(1)-O(2)	86.86 (9)	Cr(1)-O(1)-Cr(3)	89.24 (8)
O(1)-Cr(1)-O(3)	90.18 (9)	Cr(1)-O(1)-Cr(4)	93.38 (9)
O(2)-Cr(1)-O(3)	83.02 (9)	Cr(3)-O(1)-Cr(4)	97.60 (9)
O(2)-Cr(2)-O(3)	83.07 (9)	Cr(1)-O(2)-Cr(2)	97.03 (9)
O(2)-Cr(2)-O(4)	90.79 (9)	Cr(1)-O(2)-Cr(4)	92.82 (9)
O(3)-Cr(2)-O(4)	86.48 (8)	Cr(2)-O(2)-Cr(4)	88.41 (9)
O(1)-Cr(3)-O(3)	90.03 (9)	Cr(1)-O(3)-Cr(2)	96.45 (9)
O(1)-Cr(3)-O(4)	82.73 (8)	Cr(1)-O(3)-Cr(3)	88.27 (8)
O(3)-Cr(3)-O(4)	86.39 (9)	Cr(2)-O(3)-Cr(3)	93.43 (9)
O(1)-Cr(4)-O(2)	86.76 (9)	Cr(2)-O(4)-Cr(3)	93.61 (9)
O(1)-Cr(4)-O(4)	82.69 (8)	Cr(2)-O(4)-Cr(4)	87.98 (8)
O(2)-Cr(4)-O(4)	90.61 (9)	Cr(3)-O(4)-Cr(4)	96.63 (9)

[a] Cp is the centroid of the C_5H_5 ring.

Magnetic Measurements. From 4.2 to 113 K. Magnetic susceptibilities over this temperature range were determined with a Princeton Applied Research Model 155 vibrating-sample magnetometer with an applied field of 9225 G. The equipment and calibration procedures were described previously.[37] Molar magnetic susceptibilities were corrected for diamagnetism of the metal and ligands: -226×10^{-6} cm^3 mol^{-1}.[38]

From 80 to 300 K. Over this temperature range the magnetic susceptibility was measured by the Faraday method with an Alpha Scientific magnet and a Cahn electrobalance. The measurements were made by Dr. A. B. P. Lever at York University, Downsview, Ontario, Canada.

From 295 to 500 K. Over this temperature range the magnetic susceptibility was measured by the Faraday method, with a Bruker Model B-E10C8 research magnet, a Sartorius electronic microbalance, and a Bruker B-VT1000 automatic temperature controller. The measurements were made by Dr. K. Wieghardt at Ruhr Universität, Bochum, FRG.

NMR Experiments. These were performed with a Bruker CXP 200 spectrometer including a B-VT1000 variable-temperature unit. Temperature calibration was made with a Lauda R42 resistance thermometer, the sensor of which was immersed in an NMR tube containing toluene. Ferrocene was used as an internal reference and standard; $\delta^{para}(^1H)$ and $\delta^{para}(^{13}C)$ are relative to Cp_2Fe.

Photoelectron spectra were recorded on a PS 16/18 spectrometer with a heated probe and He I radiation (58.4 nm; 21.2 eV). Initial spectra were collected at 400 K. The spectrum reported was obtained at 440 K and calibrated with the known ionization potentials of MeI and Ar. No temperature dependence of the spectrum was observed.

Electronic spectra were measured in CCl_4 solution with a sealed 4-cm cell equipped with ROTAFLO joints and an O-ring for attachment to the vacuum line. The instrument used was a Perkin-Elmer 330 spectrophotometer.

Extended Hückel molecular orbital calculations used locally modified versions of the ICON8 and FORTICON8 program of Hoffmann and co-workers.[39] The parameters for H, C, and O were taken from the program; for Cr the values were as follows: exp(s) 1.7, H_{11}(s) −8.66; exp(p) 1.7, H_{11}(p) −5.24; exp(d) 4.95; expl(d) 1.80, C1 0.506, C2 0.675, H_{11}(d) −11.20.[40] In all the

(37) Haynes, J. S.; Oliver, K. W.; Rettig, S. J.; Thompson, R. C.; Trotter, J. *Can. J. Chem.* **1984**, *62*, 891.

(38) Weiss, A.; Witte, H. *Magnetochemie*; Verlag Chemie: Weinheim, FRG, 1973; pp 93–95.

(39) Howell, J.; Rossi, A.; Wallace, D.; Haraki, K.; Hoffmann, R. ICON8 and FORTICON8. *QCPE* **1977**, *11*, 344.

calculations the C–C distances in the C_5H_5 rings were 1.40 Å, the C–H 1.10 Å, the Cr–Cp 1.92 Å, and the Cr–O 1.93 Å. In the calculations on II the Cr(1)–Cr(2) distance was 3.275 Å, the Cr(1)–Cr(3), Cr(1)–Cr(4), Cr(2)–Cr(3), and Cr(2)–Cr(4) distances were averaged to 2.735 Å, and the Cr(3)–Cr(4) distance was 2.875 Å. The μ_3-η^2-C_5H_4 ligand was modeled by a HC–CH unit with a C–C distance of 1.366 Å and H–C–H angles of 112.5°.

The calculations on I were of two types. In the first type the Cr–Cr distances were varied about a mean of 2.80 Å, in order to investigate the observed distortion of I from T_d through D_{2d} to D_2 symmetry. The maximum difference in the Cr–Cr distances was 0.2 Å. In the second type of calculation the Cr–Cr distances were varied more drastically to produce different symmetries, viz. D_2, Cr(1)–Cr(2) and Cr(3)–Cr(4) 3.025, Cr(1)–Cr(4) and Cr(2)–Cr(3) 2.875, Cr(1)–Cr(3) and Cr(2)–Cr(4) 2.735 Å; D_{2d}[a], Cr(1)–Cr(2) and Cr(3)–Cr(4) 2.735, Cr(1)–Cr(3), Cr(1)–Cr(4), Cr(2)–Cr(3), and Cr(2)–Cr(4) 2.875 Å; D_{2d}[b], Cr(1)–Cr(2) and Cr(3)–Cr(4) 2.875, other Cr–Cr 2.735 Å; C_{2v}[a–d], Cr(3)–Cr(4) 2.875, Cr(1)–Cr(3), Cr(1)–Cr(4), Cr(2)–Cr(3), and Cr(2)–Cr(4) 2.735, Cr(1)–Cr(2) 2.975 (C_{2v}[a]), 3.075 (C_{2v}[b]), 3.175 (C_{2v}[c]), or 3.275 Å (C_{2v}[d]).

Results and Discussion

Preparation of $[CpCr(\mu_3\text{-}O)]_4$ (I) and $[CpCr]_4(\mu_3\text{-}\eta^2\text{-}C_5H_4)(\mu_3\text{-}O)_3$ (II). The cubane derivative II was first noticed, as a bright green cosublimate, when the residue obtained by removal of the toluene solvent from the products of the reaction between N_2O and Cp_2Cr was sublimed at 300 °C. The major portion of the sublimate was blue-black $[CpCr(\mu_3\text{-}O)]_4$ (I). Attempts to separate I and II by differential sublimation, varying the temperature and pressure, were not successful. Both I and II appear to have similar heats of sublimation. Attempts to separate blue I and green II by recrystallization were successful in the sense that the major product, I, could be purified by sacrificing II. The reverse was impossible because of the relatively low yield of II. Attempts were then made to increase the yield of II at the expense of I by varying the reaction conditions (time, temperature, and solvent). When these attempts were not successful, the oxidizing agent was varied from N_2O through O_2 and C_5H_5NO to Me_3NO. It was found that Me_3NO reproducibly gave higher yields of II relative to I. The ratio of II to I did not increase above 1:4, however, and the separation problem remained. It is not clear why Me_3NO produced a higher ratio of II compared to I than other oxidizing agents.

Chromatography of the products of the reaction between Cp_2Cr and Me_3NO was the separation technique of last resort. Despite the fact that both I and II are metal oxides, they behave in the same way as other organic derivatives of the early transition metals when subjected to column chromatography. They either are destroyed completely or can be eluted only with solvents that destroy them. We have found only two materials that can separate compounds such as I and II without extensive decomposition. One is polystyrene beads (BioBeads), which are non-polar. However, it is extremely difficult to remove all traces of water and dioxygen, which destroy both I and II, from polystyrene. The second material is 120–200 mesh glass beads. These have the advantage that they can be heated to high temperature under vacuum to remove H_2O and O_2 but the disadvantages of being polar (some I and II remain on the column and cannot be eluted) and of giving poor separation. In the present case a separation was achieved with a column of dimensions 32 × 2 cm. The solution containing Cp_2Cr, Me_3N, Me_3NO, I, II, and organic byproducts derived from C_5H_5 was loaded onto the column directly from the reaction between Cp_2Cr and Me_3NO in toluene. As the red (Cp_2Cr), blue (I), and green (II) separated, ether and then increasing amounts of THF were added; II was eluted last, with use of pure THF. The final yield of II, 2%, was acceptable because the single-step reaction could be conducted on a large scale.

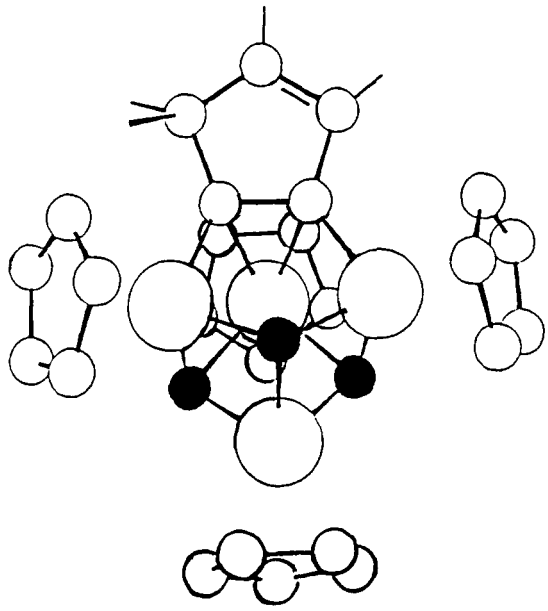

Figure 3. Structure of $[CpCr]_4(\mu_3\text{-}\eta^2\text{-}C_5H_4)(\mu_3\text{-}O)_3$ (II).

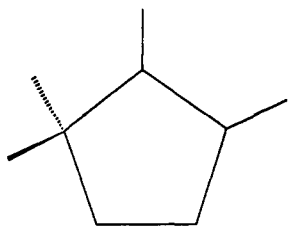

Figure 4. Structure of the η^2-C_5H_4 ligand of II.

When the structure of II (Figure 3) became known, a rational synthesis was considered. However, there is no obvious way to prepare the ligand η^2-$C_5H_4^{2-}$ with the structure shown in Figure 4. There was no reaction between I and NaCp. It is not clear how the $C_5H_4^{2-}$ ligand is formed in the reaction between Cp_2Cr and oxidizing agents. However, II was obtained reproducibly in all reactions; only the yield varied with the conditions and the oxidizing agent.

Structure of I As Determined by X-ray Diffraction. We have redetermined the structure of I at 295 and 100 K using large, multiply measured data sets (to 2θ = 70° at 295 K and to 50° at 100 K).[41] The positional parameters and derived distances are given in Tables I–IV. As is clear from the ORTEP plots in Figures 1 (295 K) and 2 (100 K), there is no disorder in the crystals. The Cr and O atoms are particularly well defined and have almost spherical thermal ellipsoids at both 295 and 100 K. At 295 K the carbon atoms C(11)–C(15), which form the η-C_5H_5 ring attached to Cr(1), have thermal parameters that are much larger than those of the other ring carbon atoms. These thermal parameters become much smaller, though still somewhat greater than those of the other rings, at 100 K (see Figures 1 and 2). We conclude that the ring attached to Cr(1) is not statically disordered but does have a

(40) Albright, T. A.; Hofmann, P.; Hoffmann, R. *J. Am. Chem. Soc.* **1977**, *99*, 7546.

(41) A data set was collected at 160 K. The structure of I derived from this was not significantly different from that at 100 K. A very restricted data set was collected at 80 K. Again, no significant difference from the structure at 100 K was noted.

Table V. Average Distances (Å) and Angles (deg) in I

param	295 K	100 K
Cr-Cr	2.8960 (5, 27)[a]	2.9012 (7, 19)
	2.8234 (5, 135)	2.8140 (7, 130)
	2.7059 (6, 55)	2.6977 (7, 27)
Cr-O	1.936 (2, 14)	1.935 (2, 16)
O-Cr-O	83.24 (7, 18)	82.88 (9, 19)
	86.30 (7, 35)	86.62 (9, 24)
	90.15 (7, 49)	90.40 (9, 39)
Cr-O-Cr	88.79 (7, 68)	88.47 (8, 76)
	93.65 (7, 50)	93.31 (9, 49)
	96.63 (7, 60)	96.93 (9, 67)

[a] The first figure is the esd and the second the maximum deviation from the mean.

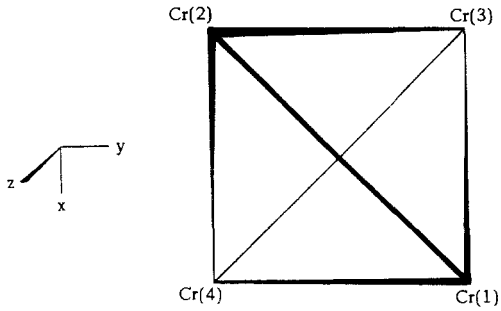

Figure 5. Numbering scheme for the Cr_4 core of $[CpCr(\mu_3\text{-}O)]_4$ and $[CpCr]_4(\mu_3\text{-}\eta^2\text{-}C_5H_4)(\mu_3\text{-}O)_3$.

high thermal motion. The following discussion of the distortion of I from T_d symmetry is only concerned with the $[Cr(\mu_3\text{-}O)]_4$ core and does not depend in any way on the Cr–C distances. Therefore, the motion of the ring attached to Cr(1) is unimportant. There is no other evidence of disorder or high thermal motion.

Examination of the distances and angles in Tables II and IV shows that there are three pairs of Cr–Cr distances, Cr–O–Cr angles, and O–Cr–O angles but only one set of 12 Cr–O distances. The pairs of Cr–Cr distances average 2.8960 (5), 2.8234 (5), and 2.7059 (6) Å at 295 K and 2.9012 (7), 2.8140 (7), and 2.6977 (7) Å at 100 K (Table V and Figure 5). There is a highly significant difference between the pairs (0.0726 (5) and 0.1175 (6) Å at 295 K, 0.0872 (7) and 0.1163 (7) Å at 100 K). The pairs of O–Cr–O angles differ by 3.06 (7) and 3.85 (7)° at 295 K and 3.74 (9) and 3.78 (9)° at 100 K. Similarly the pairs of Cr–O–Cr angles differ by 4.86 (7) and 2.98 (7)° at 295 K and 4.84 and 3.62 (9)° at 100 K. The average Cr–O distance is 1.936 (2) Å with a spread of 0.025 (2) at 295 K and 1.935 (2) Å with a spread of 0.026 (2) Å at 100 K. There are no significant trends in these distances.

Each pair of Cr–Cr distances form the opposite edges of a distorted tetrahedron of Cr atoms (Figure 5). We therefore conclude that I has D_2 symmetry to a first approximation. Closer examination suggests that I actually has C_{2v} symmetry, since the difference between the members of one of the pairs of Cr–Cr distances (that averaging 2.8234 (5) Å at 295 K and 2.8140 (7) Å at 100 K) is large compared to the esd (0.0270 (5) at 295 K and 0.0260 (5) Å at 100 K). This difference was noted in the earlier determination[24] and is therefore real. The question of D_2 or C_{2v} symmetry for I is probably not important, as is discussed below. The distortion from T_d symmetry is not due to disruption of Cr–O bonds, nor does it have any affect on these bonds, since all the Cr–O distances are equal.

There is a very minor rhombic compression of I on lowering the temperature from 295 to 100 K. Four Cr–Cr

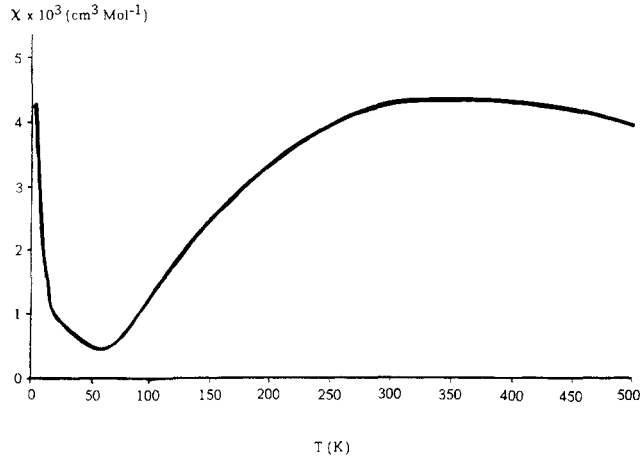

Figure 6. Plot of the bulk magnetic susceptibility (χ) of I as a function of temperature.

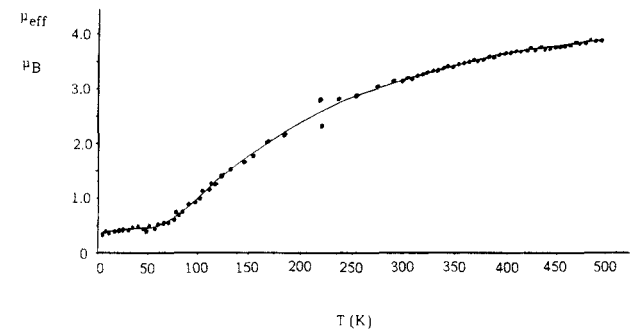

Figure 7. Plot of the effective magnetic moment of I as a function of temperature.

distances shorten (by an average of 0.0088 (6) Å) and two lengthen (by 0.0052 (6) Å). However, as Table V shows very clearly, there is no significant change in the structure or symmetry (be it D_2 or C_{2v}) of I between 295 and 100 K.

Pasynskii et al. recently determined the structure of $[Cp^1Cr(\mu_3\text{-}O)]_4$ at 293 K and found strict, crystallographically imposed, D_{2d} symmetry, with four Cr–Cr distances of 2.759 (3) Å and two of 2.896 (3) Å.[30] The Cp^1 derivative is also antiferromagnetic, with a magnetic moment of 0.60 μ_B at 77 K and 2.64 μ_B at 296 K; these values are almost identical with those of I. The diamagnetic sulfur analogue $[CpCr(\mu_3\text{-}S)]_4$ has Cr–Cr distances of 2.862 (5) and 2.854 (14), 2.891 (6) (twice), and 2.818 (3) Å (twice).[42] It has idealized and also real D_2 symmetry, although the range of distances (0.073 Å) is much smaller than in I (0.193 Å). The diamagnetic selenium analogue has four Cr–Cr distances that average 2.995 (3) Å with a range of 0.042 Å and two at 3.040 (3) Å.[30] It may be described as having idealized T_d but real C_2 symmetry. In $Cp^1{}_2Cp^5{}_2Mo_4(\mu_3\text{-}S)_4$ the average is 2.9015 (10) Å and the range 0.010 Å,[11] and in $[Cp^2Mo(\mu_3\text{-}S)]_4$ ($Cp^2 = \eta\text{-}iPrC_5H_4$; $Cp^5 = \eta\text{-}C_5Me_5$) the average is 2.894 (1) Å and the range 0.063 Å.[12] The former is both ideally and really T_d; the latter is ideally T_d and really C_2. Both $[CpMo(\mu_3\text{-}S)]_4$ compounds are diamagnetic. It is clear from these comparisons that the antiferromagnetic $[Cp'Cr(\mu_3\text{-}O)]_4$ compounds are distorted in a regular manner from T_d symmetry by amounts which are considerably beyond error limits and which are considerably greater than those of the diamagnetic S or Se analogues of Cr or Mo. The distortions are not due to steric or electronic differences between Cp, Cp^1, Cp^2, and Cp^5 ligands.[30] The distortion in I is independent of temperature.

(42) Wei, C.; Goh, L.-Y.; Bryan, R. F.; Sinn, E. *Acta Crystallogr.* **1986**, *C42*, 796.

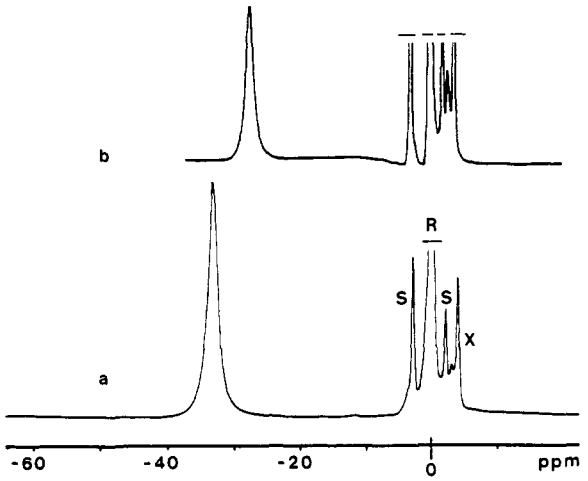

Figure 8. ^1H NMR spectra of I at (a) 386 K and (b) 217 K: S = solvent ($(^2H_8)C_6H_5CH_3$); R = reference (Cp_2Fe); X = impurity (II).

We conclude that the distortion from T_d symmetry is a real and important property of $[Cp'Cr(\mu_3\text{-}O)]_4$, compared to that for its S and Se analogues with the same number of electrons. However, the symmetry of the distorted cubane (D_2, C_{2v}, or D_{2d}) is not important and is determined by forces such as crystal packing, whose energies are two small to be considered at the level of theory that can be applied to these molecules. The distortions in $[Cp'Cr(\mu_3\text{-}O)]_4$ are much smaller than those in cubanes such as $[CpFe(\mu_3\text{-}S)]_4$, where there are two Fe–Fe distances of 2.650 (6) Å and four averaging 3.365 (6) Å.[1,2]

Magnetic Properties of I. The magnetic moment of I in the solid state was determined over the temperature range 4.2–500 K. The relevant data (χ versus T and μ_B versus T) are plotted in Figures 6 and 7. It is clear from these figures that I is antiferromagnetic. The large increase in χ below 20 K can be accounted for by approximately 0.3% Cr(III) impurity. The data indicate that I becomes diamagnetic at some temperature below 50 K. There appears to be an approach to a Néel temperature above approximately 350 K. However, I sublimes in vacuo: initial purification of I was achieved by sublimation at 500 K and 0.1 Torr; photoelectron spectra were readily obtained at 440 K and 10^{-4} Torr; mass spectra were obtained with a probe temperature of 400 K and 10^{-5} Torr. The residual pressure in the sealed tube containing the sample of I used for the determination of the magnetic moment is not accurately known but could not have been higher than 0.1 Torr. Hence, the apparent plateau in the plot of χ versus T is probably due to sublimation, which causes a change in the magnetic field of the sample.

The magnetic behavior of I was also investigated by NMR spectroscopy. As shown in Figure 8, a single ^1H signal, with a width at half-height of about 300 Hz, was observed. The shift was more than 25 ppm to high frequency from the usual diamagnetic range. This observation leads to the following conclusions. (a) The apparent symmetry of I in solution is T_d; we were unable to freeze out any species of lower symmetry down to 215 K. (b) There is unpaired electron spin density in the cluster that is sensed by the C_5H_5 ligands. (c) The electron spin relaxation is fast. The last observation is to be expected since I has an even number of electrons and is diamagnetic below 50 K. In agreement with this fast relaxation, no ESR signal was observed, in toluene, at 295 or 77 K or in the solid state at 180 K.

Since I may be viewed as a tetramer of the monomeric chromium(III) half-sandwich CpCrO, its paramagnetic ^1H NMR signal shift at the standard temperature 298 K, $\delta_{298}^{para}(^1H) = -31.56$, can be compared to those of the mononuclear compounds $CpCrX_2(L)$ (L = donor ligand), which have $\delta_{298}^{para}(^1H) < -230$.[43-46] The striking difference is due to the antiferromagnetic coupling of the electron spins in I, which is even more pronounced than for antiferromagnetic dinuclear half-sandwiches of the type $[CpCrX_2]_2$. These have $\delta_{298}^{para}(^1H)$ close to −160 ppm.[44,46] The electron exchange coupling is also evident from a temperature-dependent ^1H NMR study (details are given in the supplementary material). Figure 9 shows that the signal shift increases with temperature, whereas it should decrease for a paramagnetic species. In order to compare $\delta^{para}(^1H)$ and χ (from the solid-state measurements) at various temperatures, both are normalized to the values at 298 K, giving δ_n and χ_n.[47] When δ_n and χ_n are plotted versus T, they should give a $1/x$-type curve for paramagnetism. Figure 9 shows that I has completely different behavior, and one which is typical for antiferromagnetism.[47] Apart from some scatter in the susceptibility values, there is good agreement between the δ_n and χ_n curves. We take this as evidence that the magnetic properties are very similar in solution and in the solid state; in particular, intermolecular spin exchange is negligible over the temperature range of the NMR measurement.

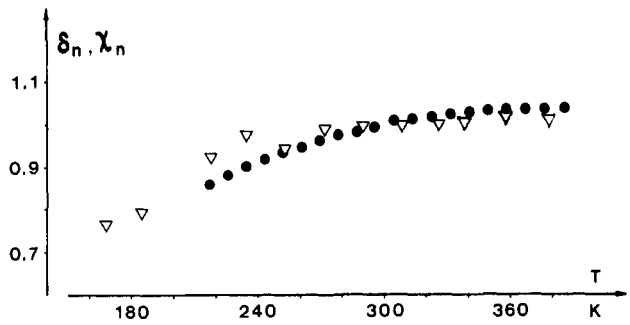

Figure 9. Normalized ^1H NMR shifts, δ_n (●), and normalized magnetic susceptibilities, χ_n (▽), of I, plotted as a function of temperature.

Good agreement between δ_n and χ_n is also expected if the NMR signal shifts are dominated by contact shifts, the signs of which depend on the electron spin delocalization. The high-frequency shift in the ^1H signal of I suggests that the metal–ligand delocalization occurs by way of electron polarization. This is similar to the case for low-spin maganocenes,[48] chromocenes, and vanadocenes[49] and is indicative of unpaired electrons residing in orbitals that have only a small ligand contribution, a fact borne out by the extended Hückel calculations discussed below. The spin delocalization of I is, however, more complicated because a ^{13}C NMR signal was found that was also shifted, even if only a small amount ($\delta_{298}^{para}(^{13}C) = -51.9$), to high frequency. This probably is due to a combination of electron polarization and σ-delocalization, as demonstrated for low-spin manganocenes.[48]

(43) Magnetic signal shifts to high frequency have a negative sign. See: Jesson, J. P. In *NMR of Paramagnetic Molecules*; La Mar, G. N., Horrocks, W. D., Jr., Holm, R. H., Eds.; Academic Press: New York, London, 1973; p 2.

(44) Köhler, F. H.; Cao, R.; Ackermann, K.; Sedlmair, J. *Z. Naturforsch., B: Anorg. Chem., Org. Chem.* **1983**, *38*, 1406.

(45) Grohmann, A.; Köhler, F. H.; Müller, G.; Zeh, H. *Chem. Ber.* **1989**, *122*, 897.

(46) Köhler, F. H.; Lachmann, J.; Müller, G.; Zeh, H.; Brunner, H.; Pfauntsch, J.; Wachter, J. *J. Organomet. Chem.* **1989**, *365*, C15.

(47) La Mar, G. N.; Eaton, G. R.; Holm, R. H.; Walker, F. A. *J. Am. Chem. Soc.* **1973**, *95*, 63.

(48) Hebendanz, N.; Köhler, F. H.; Müller, G.; Riede, J. *J. Am. Chem. Soc.* **1986**, *108*, 3281.

(49) Köhler, F. H.; Geike, W. A. *J. Organomet. Chem.* **1987**, *328*, 35.

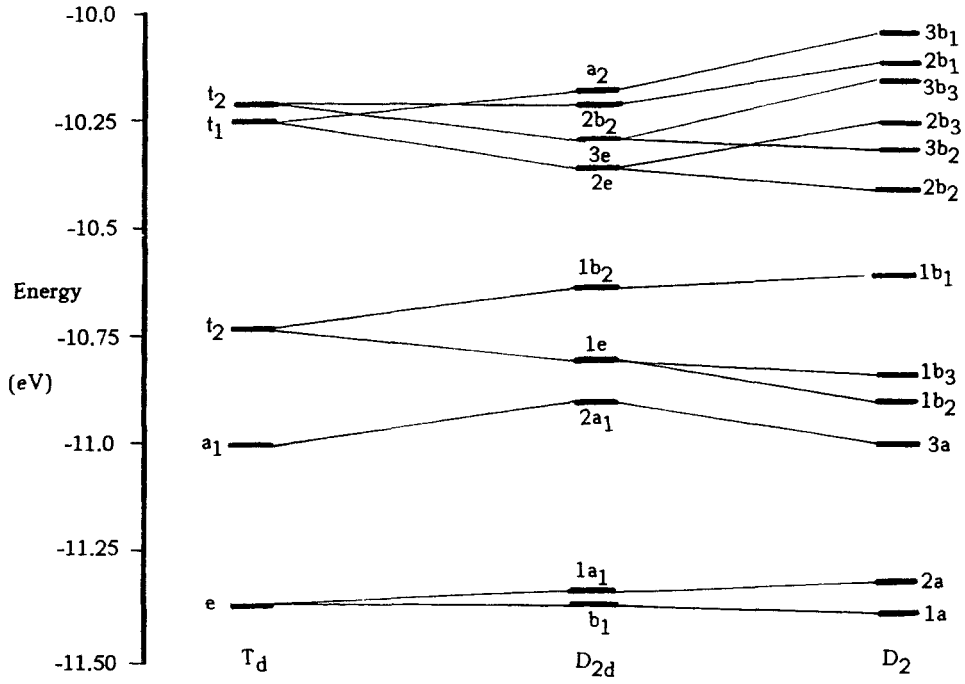

Figure 10. Energies and symmetry labels of the 12 cluster orbitals of $[CpCr(\mu_3\text{-}O)]_4$ in T_d, D_{2d}, and D_2 symmetries.

The magnetic moment of I increases from zero at below 50 K to at least 3.85 μ_B at 500 K. The increase to a moment greater than that of two unpaired electrons is only possible if at least two energy levels above the diamagnetic ground state are thermally accessible. The calculations reported below were designed to explore these higher energy levels.

Extended Hückel Molecular Orbital Calculations on I. Noniterative EHMO calculations on I have been repeated with use of standard programs,[39] and they now agree with the ordering given by Williams and Curtis for a T_d form of I.[11] The calculations have been extended to the D_{2d} geometry observed for $[Cp^1Cr(\mu_3\text{-}O)]_4$[30] and to the D_2 geometry reported here and previously[24] for I. We have also proceeded to a larger distortion of C_{2v} symmetry, since this is necessary to explain the electronic structure of II. The results for the 12 cluster orbitals in I are shown in Figure 10. As is generally agreed,[1,11,20,29] these 12 orbitals are almost pure d in character and are nonbonding with respect to the metal–carbon interaction. In the case of I they appear to be nonbonding with respect to the chromium–oxygen framework as well. This is not a general situation, since the ordering of the 12 orbitals is not the same in $[CpMo(\mu_3\text{-}S)]_4$ as it is in I.[11,12] The 12 orbitals are spread over a narrow energy range (less than 1.5 eV). For I and the related cubanes of group 6 metals combined with group 16 atoms, 12 electrons occupy these orbitals. In the relatively simple case of $[Cp'Mo(\mu_3\text{-}S)]_4$, which is diamagnetic and is of T_d symmetry, the 12 electrons just fill the e, a_1, and $1t_2$ orbitals, though the calculated order is $a_1 < e < 1t_2$ in $[CpMo(\mu_3\text{-}S)]_4$.[11] Evidence for this occupation is provided by the photoelectron spectrum of $[Cp^2Mo(\mu_3\text{-}S)]_4$,[12] which clearly shows (on the basis of band intensities) ionization of electrons from t, e, and a orbitals in increasing order of energy, with a spread that is in reasonable agreement with the EHMO calculations. For I the situation is more complicated. First, the calculations suggest that the order of the occupied orbitals in T_d symmetry is $e < a_1 < 1t_2$. Second, although I is diamagnetic at some temperature below 50 K, the onset of antiferromagnetism at very low temperature indicates that there are thermally accessible states. Third, the fact that the structure and symmetry (D_2 or C_{2v}) of I does not change between 295 and 100 K while the magnetic moment changes from 3.15 to 1.0 μ_B over this temperature range, coupled with the observation of D_{2d} symmetry for $[Cp^1Cr(\mu_3\text{-}O)]_4$ at 295 K,[30] strongly suggests that I does not have T_d symmetry at 0 K. Therefore, simple occupation of e, a_1, and $1t_2$ orbitals in a T_d molecule is not an appropriate description of I.

Two results bearing on the nature and magnitude of the distortion of I from T_d symmetry are not apparent from Figure 10. The first has been discussed by Williams and Curtis,[11] namely that, of the three occupied orbitals in T_d symmetry, only a_1 is strongly metal–metal bonding, e being weakly metal–metal bonding and $1t_2$, at least for I, being only very weakly bonding. Hence, removal of electrons from the $1t_2$ orbital will not markedly disturb any metal–metal bonding and will not lead to major changes in the metal–metal distances. This is in accord with the small magnitude of the distortion in I, where the three sets of Cr–Cr distances differ by 0.0726 (5) and 0.1175 (6) Å at 295 K, and in $[Cp^1Cr(\mu_3\text{-}O)]_4$, where the difference is 0.137 Å.[30] In contrast, removal of electrons from orbitals that are strongly metal–metal antibonding results in the differences in the Fe–Fe distances of approximately 0.75 Å observed in the $[CpFe(\mu_3\text{-}S)]_4^{n+}$ series.[1,14] An observation of relevance to the role of the a_1 orbital in metal–metal bonding is that we have obtained mass spectroscopic evidence for the existence of $[CpVO]_4$.[50] It would have the configuration $e^4a_1^21t_2^2$ (T_d symmetry). On the other hand, we have no evidence for $[CpTiO]_4$, which would have the e^4 configuration. The cubanes $[Cp^1V(\mu_3\text{-}S)]_4$, with an $a_1^2e^41t_2^2$ or $e^4a_1^21t_2^2$ configuration and a triplet ground state, and also $[Cp^1Ti(\mu_3\text{-}S)]_4$ are known.[7] The latter is diamagnetic, suggesting an e^4 rather than an $a_1^2e^2$ configuration, but has D_{2d} symmetry with two Ti–Ti distances of 2.930 (13) and four of 3.007 (10) Å.[7]

A second result bearing on the distortion of I is that depopulation of $1t_2$ and population of t_1 by any number of electrons except 3 or 6 must lead to a Jahn–Teller

(50) Bottomley, F.; Day, R. W.; Paez, D. E. Unpublished observations.

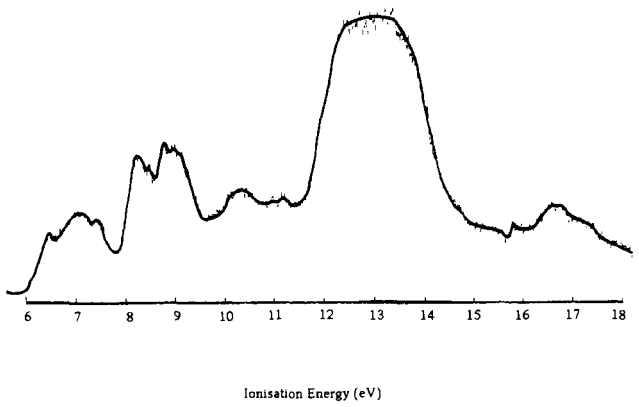

Figure 11. He I photoelectron spectrum of I. The ionization energies have an accuracy of ±0.1 eV for the broad bands.

distortion. The nature of the distortion will depend on the number of electrons in $1t_2$ and t_1. In I the number of unpaired electrons varies with temperature. If the distortion were due to a dynamic Jahn–Teller effect, it should vary with temperature, contrary to observation. The only alternative is a static distortion, i.e. that the D_{2d}, D_2, or C_{2v} structure has a lower energy than the T_d one. For I the sum of the energies of the six cluster orbitals of lowest energy (see Figure 10) is −65.959 eV for a T_d structure, −65.871 eV for D_{2d}, and −66.051 eV for D_2. The total orbital energies for the three forms are −2583.33, −2583.02, and −2583.47 eV, respectively. These energies suggest that the order of stability is $D_{2d} < T_d < D_2$. However, the differences in energy are too small to be meaningful at the extended Hückel level. Nevertheless, we believe that a static distortion driven by the energies of the various structures must be responsible for the physical properties of I and $[Cp^1Cr(\mu_3\text{-}O)]_4$.

The distortion reduces the calculated HOMO–LUMO gap quite considerably, from 0.487 eV (3900 cm^{-1}) in the T_d form to 0.203 eV (1600 cm^{-1}) in D_2 (see Figure 10). Thus, a narrowing of the gap and possible thermal promotion of electrons are favored by a distortion of I, although the magnitude of the gap is overestimated at the extended Hückel level of calculation, and the distribution of the resulting states is unknown.

He I Photoelectron Spectrum of I. The photoelectron spectrum of I is shown in Figure 11. The gas-phase structure of I is unknown, but the spectrum, recorded at 440 K, must represent that of an open-shell system, since μ is 3.8 μ_B in the solid state at this temperature. Hence, a more dense spectrum (compared to that of $[Cp^2Mo(\mu_3\text{-}S)]_4$) arises from the multiplicity of states ensuing from coupling with the open d shell. Unfortunately the ground state of I at 440 K is unknown and the complexity of the bands with low ionization energy does not enable us to apportion definitively the 12 cluster electrons, in the way that was achieved for the closed-shell $[Cp^2Mo(\mu_3\text{-}S)]_4$ species.[12] However, some general remarks can be made by considering groupings of bands, which can be assigned to certain regions. The relative tightness of the oxygen 2p orbitals implies that the spread of d-based orbitals will be less than that in the sulfur compound, where the spread is ca. 2.5 eV.[12] Indeed, we note this trend in the calculated results for $[CpCr(\mu_3\text{-}S)]_4$ and $[CpCr(\mu_3\text{-}O)]_4$.[11] We therefore assign the group of bands between 6 and 7.8 eV to ionization of the d electrons, with the sequence of ionic states unknown. The first ionization energy of $[CpCr(\mu_3\text{-}O)]_4$, 6.5 eV, is 1.5 eV higher than in $[Cp^2Mo(\mu_3\text{-}S)]_4$, which is entirely in accord with the difference between Cr and Mo, O and S, and Cp and iPrCp. In the region 8–9.7 eV, a

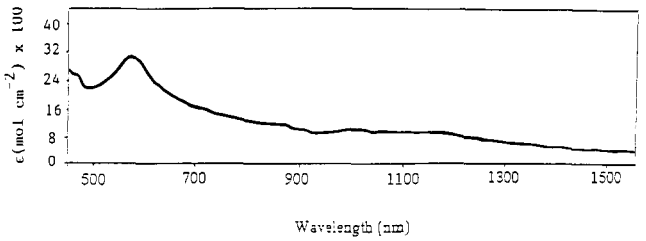

Figure 12. Electronic spectrum of I.

group of somewhat more intense bands may be assigned to ionization predominately from either the oxygen or the Cp-based ligands. Our preference is for Cp, given that such bands are observed in the He I photoelectron spectra of Cp_2Cr and related compounds.[51] This leaves the bands assignable to the oxygen ligands in the region 9.7–11.7 eV, followed by an intense band centered at 13 eV arising from Cp π and σ ionization. This assignment is in agreement with the general conclusions of the extended Hückel calculations, although no emphasis should be put on these single-configuration results in interpreting the experimental photoelectron spectrum.

The first ionization energy of I, 6.5 eV, is higher than of $[Cp^2Mo(\mu_3\text{-}S)]_4$, 5.0 eV,[12] but is still not high on an absolute scale. In accordance with this, but in contrast to a naive view of I as a simple octahedral Cr(III) derivative, I is extremely sensitive to O_2 and (though less dramatically) to H_2O. Attempts to reduce I chemically have failed.

Electronic Spectrum of I. The electronic spectrum of I, measured in CCl_4 solution at 295 K between 450 and 1550 nm (22 000–6500 cm^{-1}), is shown in Figure 12. The spectrum shows an absorption band centered at 575 nm, which is responsible for the blue color of I. This band tails gradually off into the near-infrared region, the base line never being reached. There are indications of a large number of weak bands in the 850–1500-nm region. The extinction coefficient of the absorption at 575 nm is 3150 mol cm^{-2}. Because of the difficulty in accurately weighing and manipulating the extremely air-sensitive I, the extinction coefficient is subject to large errors. Nevertheless, it is clear that the transitions responsible for the spectrum in Figure 12 are of the d–d type, in accord with the proposal that the 12 cluster orbitals are predominately metal d in character.

The energy levels as calculated by the extended Hückel method are not particularly useful for making assignments, except to indicate that a considerable number of low-energy transitions are allowed. The photoelectron spectrum shows a virtual continuum of occupied levels, and when this is coupled with the manifold of excited states arising from electronic excitation, the electronic spectrum is expected to be extremely rich. This is in agreement with the spectrum shown in Figure 12.

The picture which emerges from the photoelectron and electronic spectroscopy is that in I there is a considerable number of low-lying states, as predicted from the extended Hückel calculations; this is expected to be less so for the sulfur analogue. Specific electronic transitions cannot be handled at current levels of theoretical calculation, since a large configuration interaction would be required; nonetheless, the observed transitions are clearly of the d–d type.

Molecular Structure of II. The structure of II was determined by X-ray diffraction with sufficient accuracy to establish the geometry of the $Cr_4(\mu_3\text{-}\eta^2\text{-}C_5H_4)(\mu_3\text{-}O)_3$ core in general, and the Cr–Cr distances in particular.[28] The

(51) Green, J. C. *Struct. Bonding (Berlin)* **1981**, *43*, 37.

Table VI. Important Distances (Å) in II[a]

	molecule 1	molecule 2	av[b]
Cr(1)–Cr(2)	3.292 (10)	3.265 (10)	3.28 (1)
Cr(1)–Cr(3)	2.737 (10)	2.735 (10)	2.74 (1)
Cr(1)–Cr(4)	2.730 (10)	2.697 (8)	2.71 (9)
Cr(2)–Cr(3)	2.774 (10)	2.742 (9)	2.76 (9)
Cr(2)–Cr(4)	2.775 (12)	2.775 (12)	2.77 (1)
Cr(3)–Cr(4)	2.865 (8)	2.880 (9)	2.87 (8)
Cr–C(C_5H_4)	1.99 (5)	2.03 (4)	2.01 (5)
	2.18 (5)	2.20 (5)	2.19 (5)
Cr–O (av)	1.93 (3)	1.92 (3)	1.92 (3)
Cr–Cp (av)			1.92 (4)

[a] The structure of II is shown in Figure 3 and the numbering scheme in Figure 5. [b] Average of the two independent molecules of II in the unit cell.

structure is shown in Figure 3, and the important distances, averaged over the two independent molecules in the unit cell, are given in Table VI. The μ_3-η^2-C_5H_4 ligand (Figure 4) effectively spans the Cr(1)–Cr(2) edge of a distorted tetrahedron of chromium atoms, although the hydrocarbon ligand is also bonded to Cr(3). The Cr(1)–Cr(2) edge has lengthened markedly, to 3.28 (1) Å compared to the Cr–Cr distances of 2.70–2.90 Å in I. The opposite edge (Cr(3)–Cr(4)) is also long at 2.87 (8) Å. The other four edges average 2.74_5 (5) Å. The effect of the lengthening of the Cr(1)–Cr(2) edge, and to a lesser extent of the Cr(3)–Cr(4) edge, is to give the Cr_4 core of II idealized C_{2v} symmetry compared to D_2 (derived from T_d) for I and to reduce the Cr–Cr interaction along one edge of the tetrahedron. In this respect II resembles $[CpFe(\mu_3\text{-}S)]_4$.[1,2] However, the distortion in $[CpFe(\mu_3\text{-}S)]_4$ is caused by electronic factors, whereas in II it is imposed by the μ_3-η^2-C_5H_4 ligand. The antiferromagnetism of II (see below) is solely due to the interactions in the Cr_4 core, which depend on the Cr–Cr distances. Therefore, the cause of the distortion in the core is immaterial. The Cr–O distances in II average 1.92 (3) Å, and the Cr–Cp distances average 1.92 (4) Å, both very similar to those in I. This again indicates that the differences in the magnetic behavior of I and II are due to the different distortions of the Cr_4 core.

Magnetic Behavior of II. The magnetism of II, measured over the temperature range 4–120 K, is shown in Figure 13. Like I, II shows antiferromagnetism over this temperature range. The major difference between I and II is that whereas I becomes diamagnetic below approximately 50 K, II retains a magnetic moment to 4 K. The measured value at 4 K is 2.19 μ_B. However, as is clear from Figure 13, the magnetic moment is leveling off at approximately 2.32 μ_B at 20 K. The decrease in the magnetic moment which is observed below that temperature is probably due to traces of I being present as an impurity. The residual magnetic moment of 2.3 μ_B lies between the spin-only values for one (1.73 μ_B) and two (2.83 μ_B) unpaired electrons. This indicates that the ground state of II has two extremely closely spaced energy levels, corresponding to the HOMO–LUMO gap of a singlet–triplet cubane. Both of these are partially occupied down to 4 K.

Extended Hückel Molecular Orbital Calculations on II. In order to explain the magnetic behavior of II, and how it differs from that of I, extended Hückel calculations were performed on II and on various forms of I. The calculations were for distortion of a D_{2d} form of I, with Cr–Cr distances of 2.875 (×2) and 2.735 Å (×4), to a C_{2v} form with Cr–Cr distances of 3.275 (×1), 2.875 (×1), and 2.735 Å (×4). The details of the calculations and geometries are given in the Experimental Section. The energies and symmetries of the 12 cluster orbitals are shown graphically in Figure 14 and are given in detail in the supplementary material. The energy levels for the 12 cluster orbitals of the C_{2v} form of I, with a long Cr(1)–Cr(2) edge (3.275 Å), or for II itself, are very similar. Therefore, the results for I will be discussed, since they are easier to interpret and are of more general applicability.

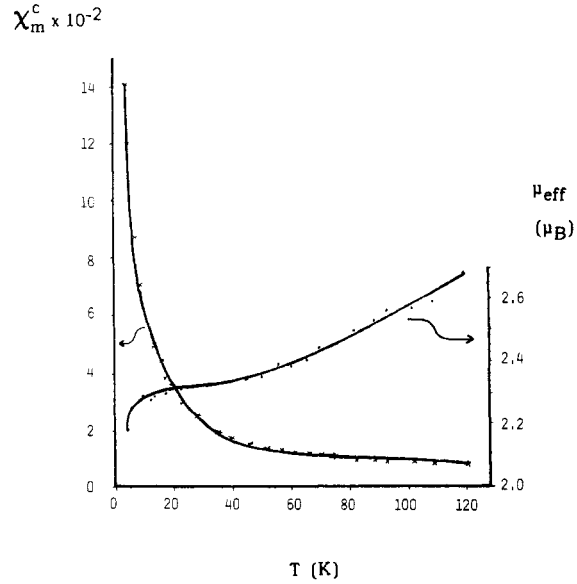

Figure 13. Magnetic behavior of II over the temperature range 4–120 K.

Because the C_{2v} and D_2 point groups contain no degenerate representations, the results for II and for I in $C_{2v}{}^d$ symmetry (Cr(1)–Cr(2) = 3.275 Å) superficially resemble those for a D_2 form of I (see Figures 10 and 14). The calculation predicts a ground state of $1a_2{}^2 1a_1{}^2 1b_1{}^2 1b_2{}^2 2a_1{}^2 2b_1{}^2 2b_2{}^0$ or $1a_2{}^2 1a_1{}^2 1b_1{}^2 1b_2{}^2 2a_1{}^2 2b_1{}^2 3a_1{}^0$ for II ($3a_1$ and $2b_2$ have the same energies, −10.4242 and −10.4260 eV). The HOMO–LUMO gap is 0.224 eV, compared to a HOMO–LUMO gap of 0.203 eV in I. This larger gap is consistent with the green color of II, compared to the blue-black color of I. Since I is diamagnetic below 50 K, II would be expected to be diamagnetic at 4 K. The real differences between the energy levels for I and for II, and the reason that II is not diamagnetic at 4 K, become clear when the distortion from the $D_{2d}{}^b$ form of I to the $C_{2v}{}^d$ form is followed (Figure 14). A D_{2d} form of I is required to be an intermediate on the way from a T_d cubane to either a D_2 or a C_{2v} distorted cubane.[52] As one goes from $D_{2d}{}^b$ to D_2 by lengthening both the Cr(1)–Cr(2) and Cr(3)–Cr(4) distances equally, the only levels that cross are either ones that will be occupied or ones that will be unoccupied. This is true even for a distortion to D_2 with Cr–Cr distances of 2.735 (×2), 2.875 (×2), and 3.025 Å (×2), which is a much larger distortion than that actually observed in I. At this point the $1b_3$ and $2b_2$ levels, representing the HOMO and LUMO of the cluster, are approximately equal in energy, and a paramagnetic ground state of $1a^2 2a^2 1b_2{}^2 1b_1{}^2 3a^2 1b_3{}^1 2b_2{}^1$ becomes possible (see the left-hand side of Figure 14). On the other hand, a small distortion from $D_{2d}{}^b$ to $C_{2v}{}^b$ by lengthening the Cr(1)–Cr(2) distance alone produces the level crossing of $2b_1$ and $3a_1$, which are the HOMO and LUMO of the cluster. A very small lengthening of Cr(1)–Cr(2) from $D_{2d}{}^b$ to $C_{2v}{}^a$ will give a (diamagnetic) ground state for I of $1a_2{}^2 1a_1{}^2 2a_1{}^2 1b_1{}^2 1b_2{}^2 3a_1{}^2 2b_1{}^0$, whereas a larger lengthening leads to the order given for II above. At a Cr(1)–Cr(2) distance calculated to be 3.04 Å, the $3a_1$ and $2b_1$ levels have the same energy. The ground state will be

(52) Jotham, R. W.; Kettle, S. F. A. *Inorg. Chim. Acta* **1971**, *5*, 183.

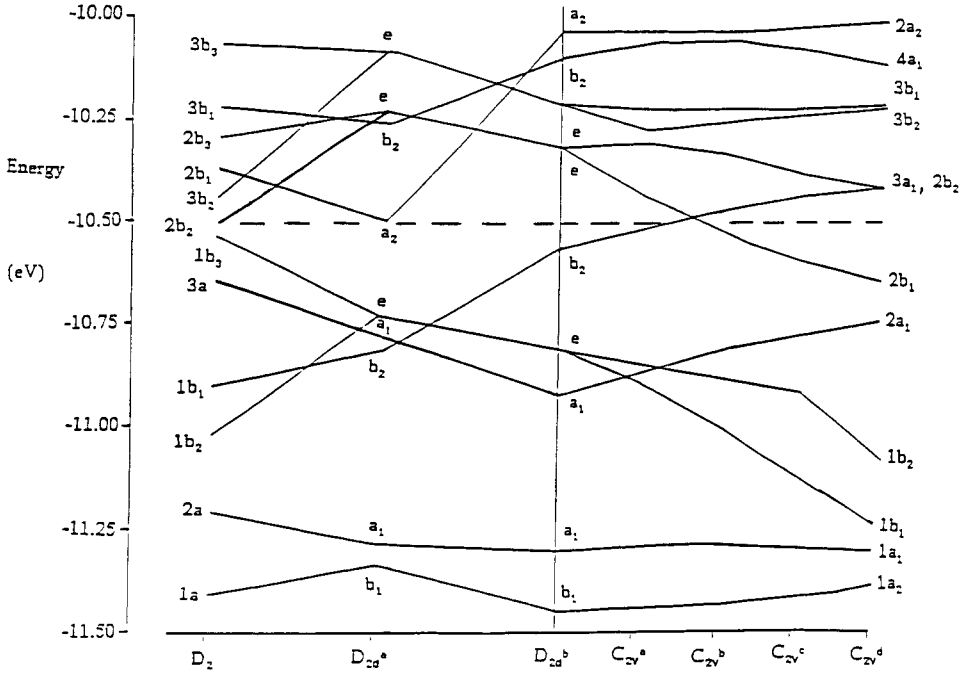

Figure 14. Energy levels for $[CpCr(\mu_3\text{-}O)]_4$ in various symmetries appropriate to II. The symmetry labels correspond to the Cr–Cr distances given in the Experimental Section.

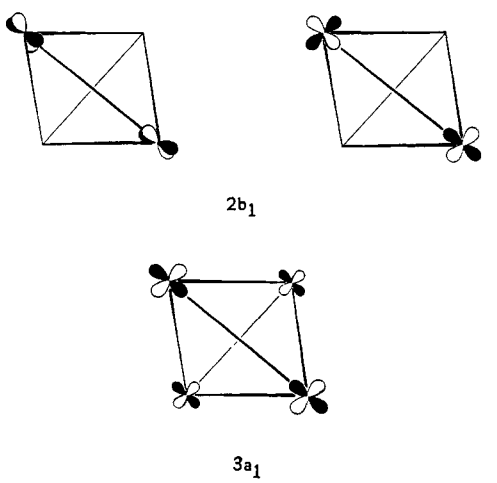

Figure 15. Contributions of the metal d orbitals to the $2b_1$ and $3a_1$ cluster orbitals of a C_{2v} form of $[CpCr(\mu_3\text{-}O)]_4$. The numbering scheme is shown in Figure 5.

$1a_2^2 1a_1^2 1b_1^2 1b_2^2 2a_1^2 2b_1^1 3a_1^1$ at this distance and at distances close to this. We suggest that this is in fact the ground state of II at 4 K.

The reason for the level crossing of $3a_1$ and $2b_1$ is that $3a_1$ is bonding with respect to the Cr(1)–Cr(2) interaction, whereas $2b_1$ is strongly antibonding. The relevant orbitals are sketched in Figure 15. The $3a_1$ orbital is also bonding between Cr(3) and Cr(4), whereas there is little contribution of any orbitals from these Cr atoms to $2b_1$. Hence, the variation in the energy of $2b_1$ shown in Figure 14 is largely independent of the Cr(3)–Cr(4) distance, but the energy of $3a_1$ is not. The same will apply to the Cr(1)–Cr(3), Cr(1)–Cr(4), Cr(2)–Cr(3), and Cr(2)–Cr(4) distances, since $3a_1$ is antibonding with respect to interactions between these four pairs of Cr atoms, whereas they make no contribution to $2b_1$.

The magnetic results indicate that the $3a_1$ and $2b_1$ orbitals have similar energies, which implies that the Cr(1)–Cr(2) distance is close to 3.04 Å, rather than the observed 3.28 Å. There are several possible reasons for this discrepancy. The magnetic moment refers to 4 K and the structural determination to 295 K. Attempts to determine the structure of II at low temperature were thwarted since the crystals crumbled on cooling. Since the Cr–Cr distances of I shorten by an average of only 0.008 Å on cooling from 295 to 100 K (Table V), thermal contraction of II could not give a Cr(1)–Cr(2) distance close to that predicted by the magnetic data and the extended Hückel calculations. The Cr–Cr distances used in the calculations were averages from the two independent molecules in the unit cell of II. The internal distances were also averaged to produce exact D_{2d} or C_{2v} symmetry. The effect of varying all six of the Cr–Cr distances as spearate entities or in concert was not attempted. The qualitative arguments on the nature of the contributions of the chromium orbitals to $2b_1$ and $3a_1$ presented above indicate that the Cr–Cr distances will have an effect on the energy of $3a_1$ and, therefore, on the crossover point. This is the probable reason for the discrepancy between the observed and calculated distances.

Chemical Properties of II. The mass spectrum of II is of interest in that ions of the type $Cp_nCr_4(C_5H_4)O_3^+$ were observed for n = 4–0, but none of the $Cp_nCr_4O_3^+$ ions appeared. The only $Cp_nCr_4O_m^+$ ion observed was $Cp_3Cr_4O_4^+$; it is believed that the latter ion was produced by oxidation of II during introduction of the sample or in the mass spectrometer. The fragmentation pattern indicates that the μ_3-η^2-C_5H_4 ligand shown in Figure 4 is extremely strongly bonded to the $Cr_4(\mu_3\text{-}O)_3$ core and effectively replaces O^{2-} of $[CpCr(\mu_3\text{-}O)]_4$. In agreement with this, II could not be reduced with chemical reducing agents. Oxidation of II with reagents containing oxygen such as N_2O, O_2, and Me_3NO yielded I in essentially quantitative yield. Water decomposed II to an unknown, insoluble, brown material.

Conclusions

The results strongly suggest that in the solid state $[CpCr(\mu_3\text{-}O)]_4$ has a symmetry which is statically distorted from T_d at all temperatures. The magnetic and spectral properties are in accord with 12 cluster orbitals of D_2 symmetry, derived by strong perturbation of those in T_d. The cluster orbitals are predominately chromium d in

character. Because of the distortion a large number of energy levels can be populated either by thermal means or by low energy radiation. Whereas $[CpCr(\mu_3\text{-}O)]_4$ is diamagnetic below 50 K, $[CpCr]_4(\mu_3\text{-}\eta^2\text{-}C_5H_4)(\mu_3\text{-}O)_3$ is paramagnetic, because two singly degenerate levels have very similar energies.

Acknowledgment. We thank Sarajane MacIntosh for assistance with the determination of the electronic spectrum of I, Professor Friedrich Grein for assistance with the molecular orbital calculations, and Professor K. Wieghardt, Ruhr Universität, Bochum, FRG, and Professor A. B. P. Lever of York University, Ontario, Canada, for magnetic measurements. The Natural Sciences and Engineering Research Council (operating grants to F.B., R.C.T., and N.P.C.W.) and the donors of the Petroleum Research Fund, administered by the American Chemical Society (operating grant to F.B.), are gratefully acknowledged for financial support.

Registry No. I, 79417-63-3; II, 99714-79-1; Cp_2Cr, 1271-24-5.

Supplementary Material Available: Tables of temperature-dependent ^1H NMR shifts and orbital energy levels, symmetries, and metal d compositions, tables of atomic parameters of hydrogen atoms, thermal parameters, all bond distances and angles, and least-squares planes at 295 and 100 K, and a drawing of I (20 pages); tables of observed and calculated structure factors for I at 295 and 100 K (46 pages). Ordering information is given on any current masthead page.

Nature of the Fe–Si Bonds in Oligosilane Complexes of the Indenyliron Dicarbonyl System: $(\eta^5\text{-}C_9H_7)Fe(CO)(L)Si_n$ (Si_n = $SiMe_3$, Si_2Me_5, 2-Si_3Me_7; L = CO, PPh_3)[1]

Keith H. Pannell,* Sheng-Hsien Lin, Ramesh N. Kapoor, Francisco Cervantes-Lee, Manuel Pinon, and Laszlo Parkanyi†

Department of Chemistry, University of Texas at El Paso, El Paso, Texas 79968-0513

Received November 7, 1989

Complexes of the general type $(\eta^5\text{-}C_9H_7)Fe(CO)(L)Si_n$ ($\eta^5\text{-}C_9H_7$ = η^5-indenyl; Si_n = $SiMe_3$, Si_2Me_5, 2-Si_3Me_7; L = CO, PPh_3) have been synthesized and characterized via X-ray crystallography. Substitution of the CO ligand by PPh_3 results in a significant increase in both the Fe–Si and Si–Si bond distances. The results rule out a significant contribution of any π-bonding to the Fe–Si bond in both the dicarbonyl and carbonyl phosphine systems and imply that steric considerations dominate the various structural changes. The η^5-indenyl groups exhibit their characteristic "slipfold" distortion, which becomes larger as the steric bulk of the other ligands increases. The synthesis of $(\eta^5\text{-}C_9H_7)Fe(CO)(L)SiMe(SiMe_3)_2$ was accomplished via photochemical rearrangement of $(\eta^5\text{-}C_9H_7)Fe(CO)_2SiMe_2SiMe_2SiMe_3$ in the presence or absence of PPh_3. ^{29}Si NMR data are in accord with the structures and previous NMR studies on silyliron complexes.

Introduction

The study of transition-metal-substituted silanes is a well-established area of organometallic chemistry due to the potential of transition metals to catalyze the reactions of organosilicon compounds, especially hydrosilylation and the formation of Si–Si bonds.[2,3] The nature of the silicon–transition-metal bond has been studied extensively, and the degree to which π-bonding between filled *n*d metal orbitals and vacant 3d silicon orbitals is important has been a matter of considerable interest. Most of the studies concerning such bonding have involved spectroscopic techniques, and the systematic structural data needed to evaluate the possibility of multiple bonding have not been available.

One series of transition-metal silyl compounds that has been well studied spectroscopically is the $(\eta^5\text{-}C_5H_5)Fe(CO)_2$–silyl system, but, since such complexes usually are oils and waxes, only a few structural studies have been published.[4] Furthermore, those few structures have not allowed a discussion of the contribution of π-bonding to the Fe–Si bond.

Chart I

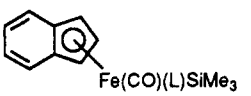

L = CO (a), PPh_3 (b); R_3Si = Me_3Si (Ia,b), Me_5Si (IIa,b), 2-$MeSi_3$ (IIIa,b)

† On leave of absence from the Central Research Institute for Chemistry of the Hungarian Academy of Sciences, Budapest, Hungary.

(1) Organometalloidal Derivatives of the Transition Metals. 25. Part 24: Sharma, H. K.; Vincenti, S. P.; Vicari, R.; Cervantes, F.; Pannell, K. H. *Organometallics* **1990**, *9*, 2109.

(2) For reviews on transition-metal silicon chemistry see: (a) Aylett, B. J. *Adv. Inorg. Chem. Radiochem.* **1982**, *25*, 1. (b) Pannell, K. H. In *Silicon Compounds Register and Review*; Anderson, R., Arkles, B., Larson, G. L., Eds.; Petrarch Systems: Bristol, PA, 1987; Vol. 4, p 32. (c) Tilley, D. J. In *Chemistry of the Functional Groups: Chemistry of Organosilicon Compounds*; Patai, S., Rappaport, Z., Eds.; Wiley: New York, 1989.

(3) For reviews on hydrosilylation see: (a) Lukevics, E.; Belyakova, Z. V. *J. Organomet. Chem. Libr.* **1977**, *5*, 1. (b) Harrod, J. F.; Chalk, A. J. In *Organic Synthesis via Metal Carbonyls*; Wender, I., Pino, P., Eds.; Wiley-Interscience: New York, 1977; Eds.; (c) Speier, J. L. *Adv. Organomet. Chem. 1979, 17*, 407.

0276-7333/90/2309-2454$02.50/0